

Configurational Prediction Of CYP2A6 Substrate Would Guide The Screening Of Potential Substrate

Received Nov. 15, 2018,
Accepted Dec. 28, 2018,

DOI: 10.4208/jams.111518.122818a

<http://www.global-sci.org/jams/>

Huizi Man^a, Yan Jia^{a,*}

Abstract. Cytochrome P450 2A6 (CYP2A6) substrate database constitute a potential class of disease related molecules as well as therapeutic molecules, primarily expressed in liver and lungs. The prediction of CYP2A6-related metabolism is of great interest. In this study, a docking protocol was presented which made use of poses of known substrate to help guide the configurational search and to rank predicted poses of test substrates. As a result, a 68% success rate was obtained. Predicting ideal configurations of compound would make significant impact on screening potential substrate, as the predicted bound conformations of 3 Tanshinone Ila(CYP2A6 substrate) analogues revealed differences among them and the inappropriate characteristic to be selected as substrates which was confirmed experimently.

1. Introduction

As high attrition rate has become a conundrum in drug development¹, the prediction of metabolism properties is of considerable interest². Cytochrome P450 (CYP) constitutes a large family of heme-containing proteins that play an important role in the oxidative metabolism of a wide variety of endogenous and exogenous compounds. Each isozyme exhibits its own, usually overlapping, substrate specificity³. The prediction of CYP-related metabolism properties finds its significance in the screening of new drugs, drug application and therapeutics with respect to drug-drug interactions, as well as patients with CYP polymorphisms⁴. Human CYP2A6 contributes extensively to nicotine detoxication but also activates tobacco-specific procarcinogens to mutagenic products⁵, as well as therapeutic drugs.

Previous works have revealed that CYP2A6 crystal structure shows a clearly well-adapted enzyme for the oxidation of small, planar substrates that can be accommodated within the compact, small, and hydrophobic active site (with a volume of only 260 Å³). Inside the active site, N297 serves as one hydrogen bond donor and thus orients ligands such as coumarin for regio-selective oxidation. Yano et al. suggest that a CH-π interaction is evident between Phe107 and coumarin or methoxsalen⁶. With the aids of this crystal structure and a pharmacophore model, Leong et al⁷ propose that Phe480 might also involve in π-π interactions of the protein with its substrates. And other active site residues such as F118 and T305 also play an important role in ligand orientation. Yet, few studies have specified the common bioactive configuration among different CYP2A6 substrates.

Except several substrate configurations available in reported CYP2A6 co-crystal structures, most biocomformations of CYP2A6 substrates in the pocket remain unknown and would only be speculated by experimentally-proved reaction site. Prediction of the bound configuration of

small-mol. ligands that differ substantially from the cognate ligand of a protein co-crystal structure is of great challenging than redocking of the cognate ligand. Here, we present a docking protocol that made use of poses of known substrate to help guide the configurational search and to rank predicted poses of test substrates. A set of 47 substrates for testing the docking protocol was tested. Overall, the top-five scoring pose family was correct over 55% of the time, with the top-ten pose families approaching a 68% success rate.

Predicting ideal configurations of compound in the pocket would make a significant impact on screening potential substrate. Lately, we have reported on the ability of CYP2A6 to accept Tanshinone Ila as high-affinity substrate⁸. In this assay, docking study revealed its bioactive configuration in the CYP2A6 pocket. Considered on the structural similarities to Tanshinone Ila, three pharmacological component Tanshinone I, Cryptotanshinone, Dihydro-tanshinone were docked into the CYP2A6 pocket. It turned out that the incoming configuration in the active site differ substantially from tanshinone Ila though sharing the same skeleton. In vitro experiment confirmed that the three mol. are not selected as substrate of CYP2A6.

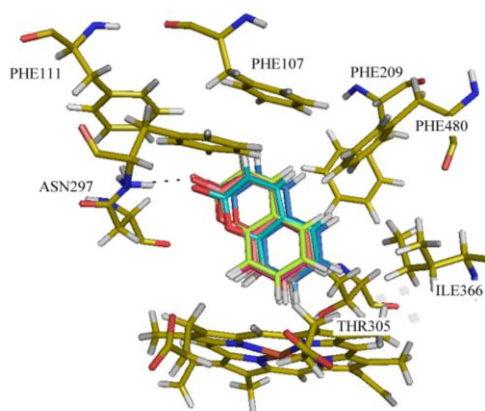


Figure 1. Binding mode of Coumarin(Top ten poses) predicted in CYP2A6 pocket versus crystal structure of Coumarin-CYP2A6 co-structure.

^aState Key Laboratory of Molecular Reaction Dynamics, Dalian Institute of Chemical Physics (DICP), Chinese Academy of Sciences (CAS), 457 Zhongshan Road, Dalian 116023, P. R. China

Corresponding author: Email: jiayan@dcp.ac.cn

2. Results and Discussion

2.1 Validation of docking simulations.

Reproducing the crystallographically observed conformation of the ligand (Coumarin) is a requirement to determine whether the docking setup is applicable to a given system. Initially, coumarin was prepared as described in the ligand preparation section (Supporting Information) and docked using the standard mode into the active site. Subsequently we compared the conformation and position with the bound ligand conformation in crystal structure measured in terms of the root-mean-square-deviation (RMSD). The top-ranked 10 poses reproduced the crystal bound conformation with a RMSD below 1 Å and the first two ranked poses had a RMSD of 0.73-0.75 Å (Figure 1). By analyzing the binding mode of first-ranked docking pose, Coumarin shows very similar interaction with residues as observed in the reported crystal structures of 1Z10, for instances, oxygen atoms of Coumarin forms hydrogen bonding with Asn297 with a distance of 2.02 Å, which in fact is smaller than the observed distance in the crystal structure (2.21 Å). As shown in the bound conformation, a favorable interaction is also evident between the pi-electron system of Phe107 and the aromatic hydrogens of coumarin10. In addition, Hydrogen bonding interaction orients coumarin for regioselective oxidation result in a distance of 3.41 Å from the hydroxylated location to the heme iron, smaller than the observed distance in the crystal structure (3.61 Å). In a word, the protocol was reliable and we would suggest it be used in predicting configurations of CYP2A6 substrates, as we have applied in the following prediction case.

2.2 Docking-based Pose prediction.

47 substrate (All molecular structures would be found in Figure S1) were obtained from literature and each molecule was prepared as described in the ligand preparation part. For each compound, 50 poses were generated and top 10 poses were used to compare with the observed configuration in reported crystal structures. If the crystal structure is not available, speculated poses with the reaction site oriented near the heme iron (guided by reported experiment result) was used.

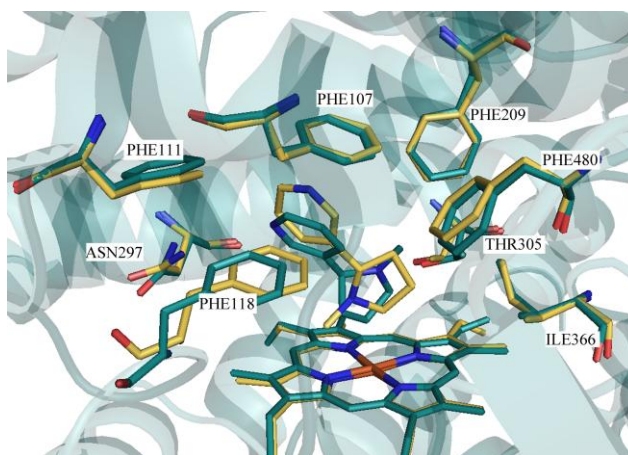


Figure 2. Binding mode of Nicotin predicted in CYP2A6 (yellow) versus crystal structure (green) of Nicotin-CYP2A6 co-structure.

When 4 similar poses out of top 10 poses (or 3 poses out of top 5 poses) consisted with the ideal configuration, we regarded it as a success prediction. 68% (55%) success rate was obtained as seen in Table S1 (Supporting Information). As is seen in the ideal bound configurations, hydrogen bonding interaction were observed between Asn297 and H-bond acceptor, eg. carbonyl oxygen atom (Cpd.1/3/5/9/10/17/31/32/33/41/43/45), ether oxygen atom (Cpd.5), furan oxygen atom (Cpd.30), hydroxyl oxygen atom (Cpd.19), pyridine nitrogen atom (Cpd.8/11/13) or imidazole nitrogen atom (Cpd.10). H-bond interaction stabilized the orientation of substrate for regioselective metabolism, which is proved by the fact that the catalytic site always lies 6-8 atoms distance from the H-bond site. These results provide further demonstration of the reliability of the docking protocol we've used, and detailed docking cases of several substrates (Nicotin, NNK, Methoxsalen, Phenacetin, Pilocarpine) which have been discussed a lot were used in comparison with observed crystal structures as below.

2.3 Binding mode of Nicotin predicted in CYP2A6 versus crystal structure of Nicotin-CYP2A6 co-structure.

CYP2A6 oxidize nicotine at several locations on the methylpyrrolidine ring. The dominant oxidation reaction for CYP2A6 is 5'-hydroxylation to form 5'-hydroxynicotine, which is further oxidized to cotinine. CYP2A6 can also oxidize nicotine on the methyl to ultimately generate nornicotine11. Consistent with this, nicotine binds with the methyl-pyrrolidine ring oriented toward the heme was observed both in the crystal structure (PDB:4EJJ. 2.30 Å) and predicted structures (Figure 2). The predicted conformation reproduced the observed conformation with an RMSD of 0.47 Å for equivalent C α positions throughout the structures, with an RMSD of 0.31 Å within the active site. In the 4EJJ complex, the pyrrolidine 5' and methyl carbons are at similar distances from the heme iron (3.4 and 5.8 Å, respectively), but the 4'-carbon is even closer at only 2.5 Å, and the pyridine nitrogen is too far (3.8 Å) from Asn-297 for even a weak hydrogen bonding interaction. In the predicted docking poses, the methyl pyrrolidine ring is oriented more vertical to the heme plane, and pyrrolidine 5'

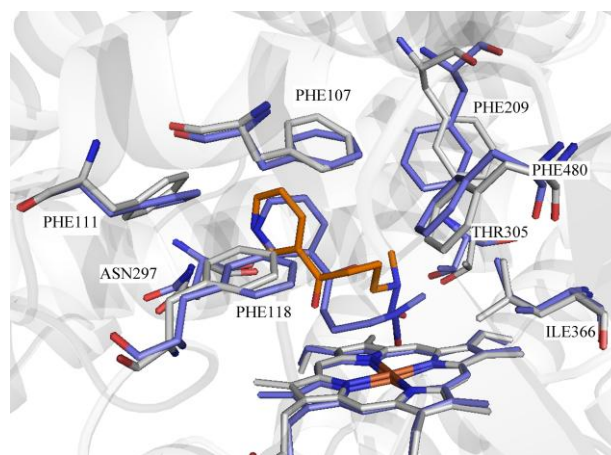


Figure 3. Binding mode of Nicotin predicted in CYP2A6 (purple) versus crystal structure (white) of Nicotin-CYP2A6 co-structure.

carbon is closer to the heme iron at only 3.35 Å, while 4' and methyl carbons are at 4.84Å and 4.57Å. The pyridine nitrogen is even far from Asn-297. Differences in the nicotine orientation are likely be mediated by several substantial differences between the two active sites determined by residues. In the 4EJJ complexes, Phe 118 is torsioned away from the active site and Phe111 slightly deviated from the heme, along with Phe480 oriented closer toward the heme, providing more space in this region compared with the protocol structure. Although the overall orientations of nicotine in the two active sites are slightly different, both emphasizes its characteristics of unable to form a hydrogen bond. And our docking poses suggest better position for 5' hydroxylation.

2.4 Binding mode of NNK predicted in CYP2A6 versus crystal structure of NNK-CYP2A13 co-structure.

NNK can be oxidized by CYP2A13 at either carbon α to the nitrosamine. The predicted pose of NNK orientations was very similar with the observed one respect to the placement of the pyridine ring, with the pyridine nitrogen serving as a hydrogen bond acceptor for Asn-29711 (Figure 3). Moreover, predicted H-bond distance(2.28 Å) was found smaller compared with observed distance of 2.8Å. The α -methylene and α -methyl carbons shows slightly closer distance of 4.62(4.63Å in 4EJH) and 4.97Å(5.24Å in 4EJH) from the heme iron. Though CYP2A13 showed slightly difference with the CYP2A6, it didn't hinder the protocol in precise prediction of NNK configuration.

Binding mode of Methoxsalen predicted in CYP2A6 versus crystal structure of Methoxsalen-CYP2A6 co-structure. The furan ring of methoxsalen was suggested to be oxidized to form an epoxide that subsequently reacts with and irreversibly inhibits the enzyme¹². The observed(PDB:1Z11, 2.05Å) and predicted complexes have an RMSD of 0.27Å for equivalent C α positions throughout the structures, and of only 0.15Å in regions associated with the active site. Methoxsalen in the predicted pocket are much like the one in the observed pocket. In the 1Z11 complex¹⁰, the furan oxygen is positioned closer to the heme iron at a distance of 3.25Å, and the nearest carbon is at 3.72Å. In the predicted docking poses, the furan oxygen is oriented closer to the heme iron at a distance of

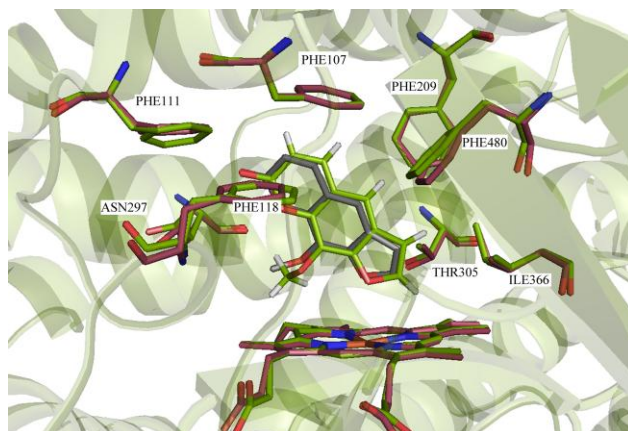


Figure 4. Binding mode of Methoxsalen predicted in CYP2A6(pink) versus crystal structure (yellow)of Methoxsalen-CYP2A6 co-structure.

3.71Å, and the nearest carbon is at 4.15Å(Figure 4). The larger methoxsalen molecule has two potential hydrogen bond acceptors, carbonyl oxygen, and alternatively the furan oxygen, but 7 out of top 10 poses(as well as reported crystal structure pose) suggest it adopts the observed single orientation probably because of additional steric constraints imposed by the active site cavity. Phe 118/111 are slightly farther from the active site in 1Z11 complex compared with docking poses, while Phe 480 is slightly nearer to the heme.

2.5 Binding mode of Phenacetin in CYP2A6 in CYP2A6 versus crystal structure of Phenacetin-CYP2A6 costructure.

Phenacetin O-Deethylation was observed in CYP2A6 wild type as well as its I208S/I300F/G301A/G369S structure. Here, the available CYP2A6 I208S/I300F/G301A/S369G in complex with Phenacetin(3EBS) 13 with resolution of 2.15Å was used to compare with the docking result. The two complexes have an RMSD of 0.396 Å for equivalent C α positions throughout the structures. In 3EBS, the hydrogen bond was clearly seen between the carbonyl oxygen of Phenacetin and Asn297, with a distance of 3.23Å. The ether oxygen of phenacetin is positioned at a distance of 4.75Å, with the nearest carbon at 4.54Å from the heme iron(Figure 5). The predicted pose showed similar conformation, but the hydrogen bond acceptor was seen 4.73 Å from Asn297, which is too far to form an H-bond. However, ether oxygen was positioned at a much closer distance of 3.16Å to the heme iron.

2.6 Binding mode of Pilocarpine in CYP2A6 in CYP2A6 versus crystal structure of pilocarpine-CYP2A6 costructure.

Pilocarpine was not only hydrolyated to 3-Hydroxypilocarpine but also competitively inhibited the activity of human CYP2A6¹⁴. The crystal structure Human CYP2A6 in complex with Pilocarpine(PDB:3T3R) was used to compare with the docking result, with an RMSD of 0.494 compared with predicted structure. In the 3T3R complexes, pilocarpine was oriented with the imidazole ring closest to the heme, with a distance of only 2.3Å from the unsubstituted nitrogen in the imidazole ring to the heme iron. The furan ring packs against the lhelix with a weak hydrogen bond from the exocyclic keto

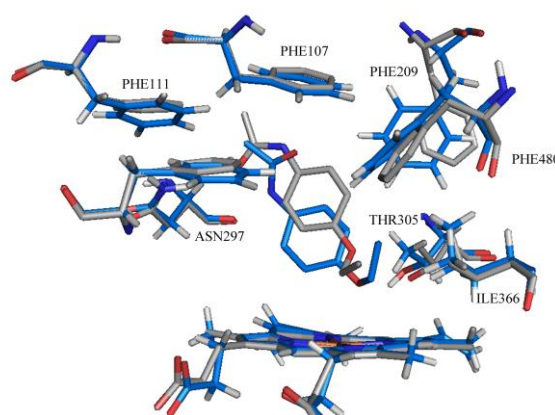


Figure 5. Binding mode of Phenacetin predicted in CYP2A6(white) versus crystal structure of Phenacetin -CYP2A6 co-structure(blue).

oxygen of pilocarpine to the Asn297 NH2 donor (3.4Å) (**Figure 6**). The ethyl group of the furan ring is directed towards Leu370. In the predicted poses, 3 out of top 10 poses suggest a similar pilocarpin pose with the superimposed furan rings and the imidazole nitrogen directed to the heme iron with a distance of only 2.07Å. However, the other 7 out of 10 predicted poses suggested furan rings oriented to the heme and a weak hydrogen bond between Asn297 and imidazole nitrogen.

2.7 Binding mode of Tanshinone IIa, Tanshinone I, Cryptotanshinone, Dihydratanshinone in CYP2A6 leads to prediction of possible substrate.

As the docking protocol has been proved to be successful in predicting the active poses of most substrate of CYP2A6, three analogues of the known substrate Tanshinone IIa, which are Tanshinone I, Cryptotanshinone, Dihydratanshinone (the structures are available in SI part) were docked into the protocol to check their potential activity. As seen in Figure 6a, top ranked poses of tanshinone IIa in the pocket were oriented with the furan oxygen directed to the hydrogen acceptor Asn297 at a distance of 2.31Å, while the active site was directed to the heme iron with a distance of 2.67Å (**Figure 7a**). This computational result turned to be in consistent with the experimental result. As a matter of fact, top 4 out of 10 poses shared the ideal conformation. Docking result for tanshinone I showed that top 9 out of 10 poses tend to orient the carbonyl oxygens closer to the heme (**Figure 7b**). For dihydratanshinone, top 5 out of 10 poses tend to orient the ether group closer to the heme, and other 5 poses follow the poses as tanshinone I (**Figure 7c**). For Cryptotanshinone, top 5 out of 10 poses tend to orient the saturated rings directed to the heme (**Figure 7d**). As a result, it turned out that, though shared the similar structure, docking studies revealed their inherent differences in interaction with proteins, and neither of the bound poses of these compounds followed the ideal poses of substrate Tanshinone IIa, which would suggest that, though insufficiently, these molecules would not be selected as CYP2A6 substrates. Slightly change in the molecule structure would cause big differences in its activity, and such docking method turned out

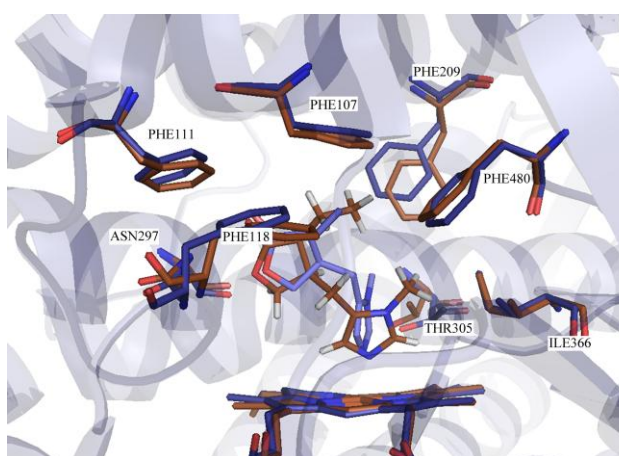


Figure 6. Binding mode of Pilocarpine predicted in CYP2A6 (orange) versus crystal structure of Pilocarpine -CYP2A6 co-structure (blue).

to be useful in predicting their potential conformations.

2.8 In vitro validation.

The four compounds were incubated in with CYP2A6 enzyme for half an hour, and then were tested with UFLC to identify whether there are any oxidized metabolites. We are excited about the result consisted with our proposal. Tanshinone IIa was oxidized to hydroxylated product Tanshinone IIb as reported¹⁵, while others showed no activity (see Figure 7). It turned out that this is a good application that in-silico method could guide the in vitro experiment. The inhibition activity of these compound against CYP2A6 were also conducted. As a result, only dihydratanshinone tend to be a moderate inhibitor (IC₅₀=1.03μM), while others showed weak inhibition activity toward CYP2A6 (>10μM). Fitness function Total Score was found to have a relationship with IC₅₀ as seen in **Table 1**, as lower score was relevant with higher IC₅₀.

3. Experimental

3.1 In-silico molecular docking studies.

3.1.1 Preparation of ligand.

The ligand was built using the ChemBioDraw version 12.0 and imported into ChemBio3D version 12.0 to generate 3D conformation. Subsequently, each mol. was read into Sybyl-X 1.1 (Tripos Inc., St Louis, MO, USA), and initial geometric optimizations were carried out using the standard Tripos force field. Gasteiger-Huckel charges were applied and all hydrogen atoms were included during the calculation. Each small molecule was saved in mol2 formats at last.

3.1.2 Preparation of Protein and Grid Generation.

The structural coordinates for CYP2A6 complexed with coumarin, were obtained from the crystal structure PDB ID: 1Z10 (with resolution of 1.90Å). The structure was prepared for docking using the Biopolymer suite of Sybyl. Chain B in 1Z10 (a tetramer) was selected to generate the corresponding protocol. Co-structures and water molecule within the model

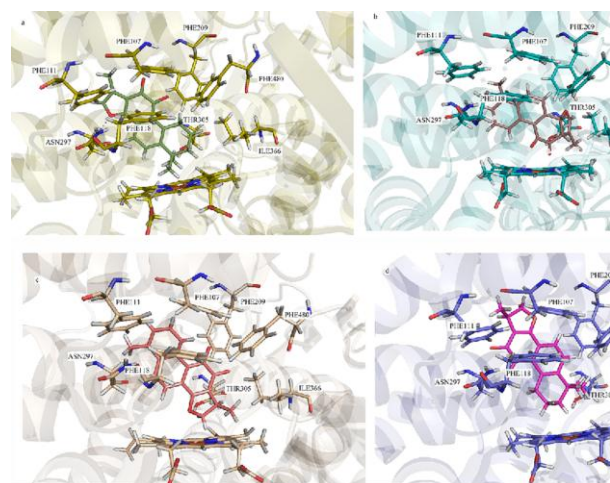


Figure 7. Binding mode of Tanshinone IIa (a), Tanshinone I (b), Dihydratanshinone (c), Cryptotanshinone (d) predicted in the CYP2A6 active pocket.

were removed and hydrogens were added, the appropriate formal charges were applied to the N- and C-termini and the structure was optimized using Tripos force field 9.

3.1.3 Ligand docking simulation.

Docking simulations of ligand were performed using the Surflex-Dock suite incorporated into Sybyl. The docking protocol (molecular space) was generated to include the residues using a 5 Å radius from the cognate ligand (Coumarin) with bloat factor = 1 and a threshold value of 0.5. For the Surflex-Dock function, the angstroms to expand search grid was set at 6 and the maximum confirmations per fragment was set to 50. The Total score fitness function was used for ranking of docking predictions and the top rankings were assessed by visual inspection.

3.1.4 Docking-based Pose prediction.

A set of 47 reported substrates were docked into the optimized protocol for testing the accuracy of docking-based pose prediction. These molecules were generated using method as ligand preparation part suggested. They were subsequently read into Sybyl and saved as a database of sln format. The database as a whole was docked into the protocol. Sybyl was used to verify the docking results and analyze the bound configuration.

3.2 Chemicals.

D-Glucose-6-phosphate, glucose-6-phosphate dehydrogenase, NADP⁺, were purchased from Sigma-Aldrich (St. Louis, MO). Tanshinone IIa, tanshinone I, cryptotanshinone, dihydrotanshinone were obtained from weikeqi Inc (Chengdu, China). CYP2A6 were obtained from BD Gentest (Woburn, MA). MgCl₂, K₂HPO₄, KH₂PO₄ were purchased from Kermel (Tianjin, China).

Table 1 Inhibition activity against CYP2A6

Compound Name	IC ₅₀ (μ M)	Total Score
Tanshinone IIa	15.3	-18.92
Tanshinone I	25.6	-11.08
Dihydrotanshinone	1.03	-10.83
Cryptotanshinone	97	-35.45

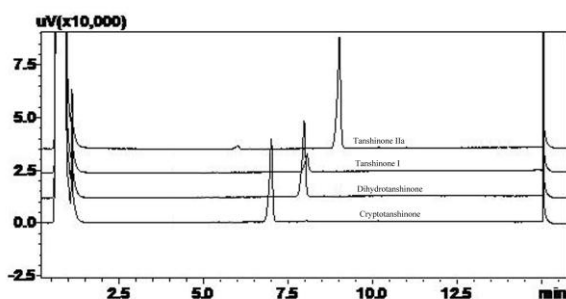


Figure 8. Representative UFLC profiles of tanshinone IIa analogs and their metabolite. All of them (200 μ M) were incubated with CYP2A6 (0.5 mg ml⁻¹) at 37°C for 30 min with (+NADP⁺) as described in the Materials and Methods section.

3.3 Enzyme study

3.3.1 Enzyme incubation.

The incubation mixture, with a total volume of 200 μ l, consisted of 100 mM potassium phosphate buffer (pH 7.4), an NADPH-generating system (1 mM NADP⁺, 10 mM glucose-6-phosphate, 1 U/ml glucose-6-phosphate dehydrogenase, and 4 mM MgCl₂), CYP2A6(0.5 mg/ml), and 100 μ M Tanshinones (including Tanshinone IIa, Tanshinone I, Cryptotanshinone, Dihydrotanshinone). The reaction was initiated by adding the NADPH-generating system. After incubation for 30 min in a shaking water bath, the reaction was terminated by the addition of acetonitrile (200 μ l). The mixture was kept on ice until it was centrifuged at 20,000g for 10 min at 4 °C. Aliquots of supernatants were transferred for UFLC analysis. Control incubations without NADPH or without substrate or without CYP2A6 were carried out to ensure that metabolite formation was NADPH-dependent. Aliquots of supernatants were analyzed by a UFLC spectrometry system. (Shimadzu, Kyoto, Japan), equipped with two LC-20AD pumps, a DGU-20A3 vacuum degasser, a SIL-20AHT autosampler, a CTO-20AC column oven, an SPD-M 20A DAD, a CBM-20A communications bus module, a mass detector (2010EV) with an electrospray ionization (ESI) interface, and a computer equipped with UFLC-MS solution software (version 3.41; Shimadzu). A Shim-pack XR-ODS (75.0 \times 2.0 mm i.d., 2.2 μ m; Shimadzu) analytical column with an ODS guard column (5 \times 2.0 mm i.d., 2.2 μ m; Shimadzu) was used to separate Tanshinones and their metabolites. Column temperature was kept at 40°C. The mobile phase was acetonitrile (A) and 0.2% formic acid (B) at a flow rate of 0.3 ml/min, with the following gradient: 0 to 9 min, 70% B to 5% B; 9 to 12.5 min, 5% B; and 12.5 to 16 min, balance to 70% B. They were detected at the detector wavelength of 270 nm with an ESI interface both in positive and negative ion mode (ESI⁻) from m/z 100 to 800. The detector voltage was set at +1.55 kV and -1.55 kV for positive and negative ion detection, respectively.

3.3.2 Enzyme inhibition study.

The incubation mixture, with a total volume of 200 μ l, consisted of 100 mM potassium phosphate buffer (pH 7.4), an NADPH-generating system (1 mM NADP⁺, 10 mM glucose-6-phosphate, 1 U/ml glucose-6-phosphate dehydrogenase, and 4 mM MgCl₂), CYP2A6(0.5 mg/ml), and a series of different concentrations of Tanshinones (as inhibitor, including Tanshinone IIa, Tanshinone I, Cryptotanshinone, Dihydrotanshinone) and 2 μ M coumarin(as substrate). The reaction was initiated by adding the NADPH-generating system. After incubation for 30 min in a shaking water bath, the reaction was terminated by the addition of acetonitrile (200 μ l). UFLC analysis was applied as describe above.

4. Conclusions

A docking protocol made use of poses of known ligands was generated and used in predicting the ideal conformations of 47 reported CYP2A6 substrates in the pocket. Predicting of the bound configurations of these compounds that differ

substantially from the cognate ligand (coumarin) approached an approximately 68% success rate. The specified protocol would be used in predicting CYP2A6 substrate out of similar structures, as the bound configurations of three Tanshinone IIA (known CYP2A6 substrate) analogues did not suggest them as substrate of CYP2A6, which was verified by the in vitro experiment. This method could be further expanded for qualitative predictions of drug metabolism mediated by CYP2A6 helping to develop drugs.

Acknowledgements

This work was supported by the National Natural Science Foundation of China (21703245).

References

- [1] Kola, I.; Landis, J., Can the pharmaceutical industry reduce attrition rates? *Nature Reviews Drug Discovery* 2004, 3 (8), 711-715.
- [2] Wienkers, L. C.; Heath, T. G., Predicting in vivo drug interactions from in vitro drug discovery data. *Nature Reviews Drug Discovery* 2005, 4 (10), 825-833.
- [3] Dong, D.; Wu, B.; Chow, D.; Hu, M., Substrate selectivity of drug-metabolizing cytochrome P450s predicted from crystal structures and in silico modeling. *Drug metabolism reviews* 2012, 44 (2), 192-208.
- [4] Lee, I. S.; Kim, D., Polymorphic metabolism by functional alterations of human cytochrome P450 enzymes. *Archives of pharmacol research* 2011, 34 (11), 1799-816.
- [5] a. Yamazaki, H.; Inoue, K.; Hashimoto, M.; Shimada, T., Roles of CYP2A6 and CYP2B6 in nicotine C-oxidation by human liver microsomes. *Arch Toxicol* 1999, 73 (2), 65-70; b. Patten, C. J.; Smith, T. J.; Murphy, S. E.; Wang, M. H.; Lee, J.; Tynes, R. E.; Koch, P.; Yang, C. S., Kinetic analysis of the activation of 4-(methylnitrosamino)-1-(3-pyridyl)-1-butanone by heterologously expressed human P450 enzymes and the effect of P450-specific chemical inhibitors on this activation in human liver microsomes. *Arch Biochem Biophys* 1996, 333 (1), 127-138.
- [6] Chougnat, A.; Woggon, W. D.; Locher, E.; Schilling, B., Synthesis and in vitro activity of heterocyclic inhibitors of CYP2A6 and CYP2A13, two cytochrome P450 enzymes present in the respiratory tract. *Chembiochem : a European journal of chemical biology* 2009, 10 (9), 1562-7.
- [7] Leong, M. K.; Chen, Y. M.; Chen, H. B.; Chen, P. H., Development of a New Predictive Model for Interactions with Human Cytochrome P450 2A6 Using Pharmacophore Ensemble/Support Vector Machine (PhE/SVM) Approach. *Pharmaceutical research* 2009, 26 (4), 987-1000.
- [8] Liu, H. X.; Hu, Y.; Liu, Y.; He, Y. Q.; Li, W.; Yang, L., Hydroxylation of tanshinone IIA in human liver microsomes is specifically catalysed by cytochrome P4502A6. *Xenobiotica; the fate of foreign compounds in biological systems* 2009, 39 (5), 382-390.
- [9] Co., N.-H. P., *Mathematical Programming* 1997, 12 (241).
- [10] Pelkonen, O.; Rautio, A.; Raunio, H.; Pasanen, M., CYP2A6: a human coumarin 7-hydroxylase. *Toxicology* 2000, 144 (1-3), 139-147.
- [11] DeVore, N. M.; Scott, E. E., Nicotine and 4-(methylnitrosamino)-1-(3-pyridyl)-1-butanone binding and access channel in human cytochrome P450 2A6 and 2A13 enzymes. *J Biol Chem* 2012, 287 (32), 26576-85.
- [12] Koenigs, L. L.; Trager, W. F., Mechanism-based inactivation of P450 2A6 by furanocoumarins. *Biochemistry* 1998, 37 (28), 10047-61.
- [13] DeVore, N. M.; Smith, B. D.; Urban, M. J.; Scott, E. E., Key Residues Controlling Phenacetin Metabolism by Human Cytochrome P450 2A Enzymes. *Drug Metab Dispos* 2008, 36 (12), 2582-2590.
- [14] DeVore, N. M.; Meneely, K. M.; Bart, A. G.; Stephens, E. S.; Battaile, K. P.; Scott, E. E., Structural comparison of cytochromes P450 2A6, 2A13, and 2E1 with pilocarpine. *The FEBS journal* 2012, 279 (9), 1621-31.
- [15] Gillam, E. M.; Notley, L. M.; Cai, H.; De Voss, J. J.; Guengerich, F. P., Oxidation of indole by cytochrome P450 enzymes. *Biochemistry* 2000, 39 (45), 13817-24.
- [16] Kimura, M.; Yamazaki, H.; Fujieda, M.; Kiyotani, K.; Honda, G.; Saruwatari, J.; Nakagawa, K.; Ishizaki, T.; Kamataki, T., CYP2A6 is a principal enzyme involved in hydroxylation of 1,7-dimethylxanthine, a main caffeine metabolite, in humans. *Drug Metab Dispos* 2005, 33 (9), 1361-1366.
- [17] Reigh, G.; McMahon, H.; Ishizaki, M.; Ohara, T.; Shimane, K.; Esumi, Y.; Green, C.; Tyson, C.; Ninomiya, S., Cytochrome P450 species involved in the metabolism of quinoline. *Carcinogenesis* 1996, 17 (9), 1989-1996.
- [18] Shimada, T.; Tsumura, F.; Yamazaki, H., Prediction of human liver microsomal oxidations of 7-ethoxycoumarin and chlorzoxazone with kinetic parameters of recombinant cytochrome P-450 enzymes. *Drug Metab Dispos* 1999, 27 (11), 1274-1280.
- [19] Li, D. M.; Huang, X. Q.; Han, K. L.; Zhan, C. G., Catalytic Mechanism of Cytochrome P450 for 5'-Hydroxylation of Nicotine: Fundamental Reaction Pathways and Stereoselectivity. *J Am Chem Soc* 2011, 133 (19), 7416-7427.
- [20] Nakajima, M.; Yamamoto, T.; Nunoya, K.; Yokoi, T.; Nagashima, K.; Inoue, K.; Funae, Y.; Shimada, N.; Kamataki, T.; Kuroiwa, Y., Characterization of CYP2A6 involved in 3'-hydroxylation of cotinine in human liver microsomes. *The Journal of pharmacology and experimental therapeutics* 1996, 277 (2), 1010-5.
- [21] Nunoya, K. I.; Yokoi, T.; Kimura, K.; Kodama, T.; Funayama, M.; Inoue, K.; Nagashima, K.; Funae, Y.; Shimada, N.; Green, C.; Kamataki, T., (+)-cis-3,5-dimethyl-2-(3-pyridyl) thiazolidin-4-one hydrochloride (SM-12502) as a novel substrate for cytochrome P450 2A6 in human liver microsomes. *Journal of Pharmacology and Experimental Therapeutics* 1996, 277 (2), 768-774.
- [22] Ikeda, K.; Yoshisue, K.; Matsushima, E.; Nagayama, S.; Kobayashi, K.; Tyson, C. A.; Chiba, K.; Kawaguchi, Y., Bioactivation of tegafur to 5-fluorouracil is catalyzed by cytochrome P-450 2A6 in human liver microsomes in vitro. *Clinical Cancer Research* 2000, 6 (11), 4409-4415.
- [23] Xu, Y.; Shen, Z.; Shen, J.; Liu, G.; Li, W.; Tang, Y., Computational insights into the different catalytic activities of CYP2A13 and CYP2A6 on NNK. *Journal of molecular graphics & modelling* 2011, 30, 1-9.
- [24] Patten, C. J.; Smith, T. J.; Friesen, M. J.; Tynes, R. E.; Yang, C. S.; Murphy, S. E., Evidence for cytochrome P450 2A6 and 3A4 as major catalysts for N'-nitrososornicotine alpha-hydroxylation by human liver microsomes. *Carcinogenesis* 1997, 18 (8), 1623-1630.
- [25] Kamataki, T.; Fujita, K.; Nakayama, K.; Yamazaki, Y.; Miyamoto, M.; Ariyoshi, N., Role of human cytochrome P450 (CYP) in the metabolic activation of nitrosamine derivatives: Application of genetically engineered Salmonella expressing human CYP. *Drug metabolism reviews* 2002, 34 (3), 667-676.
- [26] Wong, H. L.; Murphy, S. E.; Hecht, S. S., Cytochrome P450 2A-catalyzed metabolic activation of structurally similar carcinogenic nitrosamines: N'-nitrososornicotine enantiomers, N-nitrosopiperidine, and N-nitrosopyrrolidine. *Chemical research in toxicology* 2005, 18 (1), 61-9.

- [27] Liu, C.; Zhuo, X. L.; Gonzalez, F. J.; Ding, X. X., Baculovirus-Mediated expression and characterization of rat CYP2A3 and human CYP2A6: Role in metabolic activation of nasal toxicants. *Mol Pharmacol* 1996, 50 (4), 781-788.
- [28] a. Miyazawa, M.; Marumoto, S.; Takahashi, T.; Nakahashi, H.; Haigou, R.; Nakanishi, K., Metabolism of (+)- and (-)-menthols by CYP2A6 in human liver microsomes. *J Oleo Sci* 2011, 60 (3), 127-32. b. Miyazawa, M.; Gyoubu, K., Metabolism of (-)-fenchone by CYP2A6 and CYP2B6 in human liver microsomes. *Xenobiotica; the fate of foreign compounds in biological systems* 2007, 37 (2), 194-204. c. Miyazawa, M.; Gyoubu, K., Metabolism of (+)-fenchone by CYP2A6 and CYP2B6 in human liver microsomes. *Biol Pharm Bull* 2006, 29 (12), 2354-8. d. Gyoubu, K.; Miyazawa, M., In vitro metabolism of (-)-camphor using human liver microsomes and CYP2A6. *Biol Pharm Bull* 2007, 30 (2), 230-233. e. Miyazawa, M.; Sugie, A.; Shimada, T., Roles of human CYP2A6 and 2B6 and rat CYP2C11 and 2B1 in the 10-hydroxylation of (-)-verbenone by liver microsomes. *Drug Metab Dispos* 2003, 31 (8), 1049-1053.
- [29] Hong, J. Y.; Wang, Y. Y.; Bondoc, F. Y.; Lee, M.; Yang, C. S.; Hu, W. Y.; Pan, J. M., Metabolism of methyl tert-butyl ether and other gasoline ethers by human liver microsomes and heterologously expressed human cytochromes P450: Identification of CYP2A6 as a major catalyst. *Toxicology and applied pharmacology* 1999, 160 (1), 43-48.
- [30] Kharasch, E. D.; Hankins, D. C.; Fenstamaker, K.; Cox, K., Human halothane metabolism, lipid peroxidation, and cytochromes P(450)2A6 and P(450)3A4. *Eur J Clin Pharmacol* 2000, 55 (11-12), 853-859.
- [31] Murai, K.; Yamazaki, H.; Nakagawa, K.; Kawai, R.; Kamataki, T., Deactivation of anti-cancer drug letrozole to a carbinol metabolite by polymorphic cytochrome P450 2A6 in human liver microsomes. *Xenobiotica; the fate of foreign compounds in biological systems* 2009, 39 (11), 795-802.
- [32] a. Torchin, C. D.; McNeilly, P. J.; Kapetanovic, I. M.; Strong, J. M.; Kupferberg, H. J., Stereoselective metabolism of a new anticonvulsant drug candidate, losigamone, by human liver microsomes. *Drug Metab Dispos* 1996, 24 (9), 1002-1008. b. White, I. N., A continuous fluorometric assay for cytochrome P-450-dependent mixed function oxidases using 3-cyano-7-ethoxycoumarin. *Anal Biochem* 1988, 172 (2), 304-10. c. Niwa, T.; Shiraga, T.; Yamasaki, S.; Ishibashi, K.; Ohno, Y.; Kagayama, A., In vitro activation of 7-benzoyloxyresorufin O-debenzylation and nifedipine oxidation in human liver microsomes. *Xenobiotica; the fate of foreign compounds in biological systems* 2003, 33 (7), 717-29. d. Ohno, Y.; Kawanishi, T.; Takahashi, A.; Kasuya, Y.; Omori, Y., Renal Drug-Metabolism .1. Species-Differences of Cyt-P450 and Demethylation of Aminopyrine and N-Nitrosodimethylamine. *Jpn J Pharmacol* 1980, 30, P63-P63. e. Roy, P.; Yu, L. J.; Crespi, C. L.; Waxman, D. J., Development of a substrate-activity based approach to identify the major human liver P-450 catalysts of cyclophosphamide and ifosfamide activation based on cDNA-expressed activities and liver microsomal P-450 profiles. *Drug Metab Dispos* 1999, 27 (6), 655-66. f. Benetton, S. A.; Fang, C.; Yang, Y. O.; Alok, R.; Year, M.; Lin, C. C.; Yeh, L. T., P450 phenotyping of the metabolism of selegiline to desmethylselegiline and methamphetamine. *Drug Metab Pharmacol* 2007, 22 (2), 78-87. h. Satoh, T.; Fujita, K.; Munakata, H.; Itoh, S.; Nakamura, K.; Kamataki, T.; Itoh, S.; Yoshizawa, I., Studies on the interactions between drugs and estrogen: Analytical method for prediction system of gynecomastia induced by drugs on the inhibitory metabolism of estradiol using *Escherichia coli* coexpressing human CYP3A4 with human NADPH-cytochrome P450 reductase. *Anal Biochem* 2000, 286 (2), 179-186. i. Schmidt, R.; Baumann, F.; Hanschmann, H.; Geissler, F.; Preiss, R., Gender difference in ifosfamide metabolism by human liver microsomes. *European journal of drug metabolism and pharmacokinetics* 2001, 26 (3), 193-200. j. Yun, C. H.; Shimada, T.; Guengerich, F. P., Purification and Characterization of Human Liver Microsomal Cytochrome-P-450 2a6. *Mol Pharmacol* 1991, 40 (5), 679-685. k. Lee, S. H.; Slattery, J. T., Cytochrome P450 isozymes involved in isofylline metabolism to pentoxifylline in human liver microsomes. *Drug Metab Dispos* 1997, 25 (12), 1354-8. l. Saleh, S.; Johnston, A.; Turner, P., Measurement of medifoxamine metabolites in urine by high-performance liquid chromatography. *Journal of chromatography* 1990, 528 (2), 531-6. m. Yano, J. K.; Hsu, M. H.; Griffin, K. J.; Stout, C. D.; Johnson, E. F., Structures of human microsomal cytochrome P450 2A6 complexed with coumarin and methoxsalen. *Nature structural & molecular biology* 2005, 12 (9), 822-3. n. Stresser, D. M.; Kupfer, D., Human cytochrome P450-catalyzed conversion of the proestrogenic pesticide methoxychlor into an estrogen - Role of CYP2C19 and CYP1A2 in O-demethylation. *Drug Metab Dispos* 1998, 26 (9), 868-874. o. Furge, L. L.; Fletke, K. J., HPLC determination of caffeine and paraxanthine in urine - An assay for cytochrome P450 1A2 activity. *Biochem Mol Biol Edu* 2007, 35 (2), 138-144. p. Niwa, T.; Yabusaki, Y.; Honma, K.; Matsuo, N.; Tatsuta, K.; Ishibashi, F.; Katagiri, M., Contribution of human hepatic cytochrome P450 isoforms to regioselective hydroxylation of steroid hormones. *Xenobiotica; the fate of foreign compounds in biological systems* 1998, 28 (6), 539-47. q. Stanjek, V.; Miksch, M.; Lueer, P.; Matern, U.; Boland, W., Biosynthesis of psoralen: Mechanism of a cytochrome p450 catalyzed oxidative bond cleavage. *Angew Chem Int Edit* 1999, 38 (3), 400-402.